Switchable half-metallicity in A-type antiferromagnetic NiI2 bilayer coupled with ferroelectric In2Se3

Yanlu Li (liyanlu@sdu.edu.cn)
Shandong University
Yaping Wang
Shandong University
Xinguang Xu
Shandong University
Xian Zhao
Shandong University
Weixiao Ji
University of Jinan
Qiang Cao
University of Jinan
Shengshi Li
University of Jinan

Article

Keywords:

Posted Date: June 6th, 2022

DOI: https://doi.org/10.21203/rs.3.rs-1675184/v1

Version of Record: A version of this preprint was published at npj Computational Materials on October 23rd, 2022. See the published version at https://doi.org/10.1038/s41524-022-00904-6.

Switchable half-metallicity in A-type antiferromagnetic NiI_2 bilayer coupled with ferroelectric In_2Se_3

Yaping Wang[1], Xinguang Xu[1], Xian Zhao[2], Weixiao Ji[3], Qiang Cao[3], Shengshi Li[3*] and Yanlu Li[1*]

1 *State Key Lab of Crystal Materials and Institute of Crystal Materials, Shandong University, Jinan 250100, China*

2 *Center for Optics Research and Engineering of Shandong University, Shandong University, Qingdao 266237, China*

3 *Spintronics Institute, University of Jinan, Jinan, 250022, China*

* *Corresponding authors*

Abstract

Electrically induced and controlled half-metallicity or fully spin polarized current in antiferromagnet is of great significance for both fundamental research and practical application in spintronics. Here, by combining two-dimensional (2D) A-type antiferromagnetic (AFM) NiI_2 bilayer (bi-NiI_2) with ferroelectric (FE) In_2Se_3 with different thickness to construct van der Waals (vdW) heterostructure, we propose that the AFM half-metallicity is realizable and switchable in the bi-NiI_2 proximate to In_2Se_3 bilayer (bi-In_2Se_3). The reversal of the electric polarization of the FE bi-In_2Se_3 successfully drives nonvolatile transition between half-metal and semiconductor for the AFM bi-NiI_2. The mechanism of this intriguing phenomenon cooperatively stems from the energy band shift driven by the polarization field, and from the interfacial charge transfer. Besides, the easy magnetization axis of the bi-NiI_2 is switched between the out-of-plane and in-plane directions for the two opposite polarization states. More interestingly, by introducing strain, the half-metallic behavior and magnetic anisotropy energy (MAE) of the bi-NiI_2 in the heterostructure can be effectively manipulated. These findings provide not only a feasible strategy for nonvolatile electrical controlled half-metallicity in a 2D antiferromagnet, but also a promising platform for designing new advanced nanodevices.

1. Introduction

Antiferromagnetic (AFM) spintronics,[1-3] as a frontier area of research, is expected to bring about the revolutionary progress for the next-generation spintronic devices. This is because the antiferromagnets possess various fascinating features, such as robustness against external magnetic field perturbation, absence of parasitic stray field, and ultrafast dynamics.[4-7] To utilize AFM materials as the active elements in spintronics, several key issues remain to be resolved, in which the generation and manipulation of half-metallicity or fully spin polarized current are very important aspects.[8] Achieving the half-metallicity through the electric field has been pursued recently,[9] due to the unique superiority of low power and fast response, and it is conducive to the implementation of fully electrical reading/writing.[10] Recently, the long sought electric field controlled half-metallicity was predicted in two-dimensional (2D) A-type AFM VSe_2 bilayer which features with intralayer ferromagnetic (FM) and interlayer AFM couplings.[11] However, the achieved half-metallicity is volatile, since the fully spin polarized conduction electron would dissipate with the removal of the electric field, which is less desirable for memory and logic devices. As a result, it is urgently required a practical scheme for a nonvolatile electrical controlled half-metallicity.

Recently, van der Waals (vdW) heterostructure has attracted extensive attention for both fundamental science and technological application,[12-14] which offers a platform to realize intriguing physics and functionalities by flexibly stacking layered material with various properties. One of the most representative examples is the multiferroic vdW heterostructure constructed based on 2D FM and ferroelectric (FE) materials, which shows a strong interfacial magnetoelectric effect, such as FE controlled half-metallicity and magnetic order. [15-20] The FE layer, on the one hand, is to provide a spontaneous polarization field, which enables the control of the electronic or magnetic properties of FM layer. On the other hand, the FE layer holds different work functions at two surfaces, which diversifies the interfacial charge transfer with the reversal of the electric polarization, providing an effective avenue for band structure engineering. Motivated by such a principle, here we propose that the half-metallicity in 2D A-type antiferromagnet can be achieved by introducing a FE substrate with out-of-plane electric polarization to construct a multiferroic heterostructure. Figure 1a presents a schematic illustration of spin- and layer-resolved density of state (DOS) for an A-type AFM bilayer.

Although there is no spin polarization in the total DOS, the inherent ferromagnetism of monolayer makes the different spin subbands locate on different monolayer spatially. Such a characteristic provides an opportunity to realize the half-metallicity by breaking the inversion symmetry. When the 2D A-type antiferromagnet is deposited on a FE substrate, shown in Figure 1b, the presence of the polarization field and possible interfacial charge transfer due to work function difference are expected to trigger the different electrostatic potential between two FM layers. In this context, the DOS associated with layer-1 will be shifted downwards with respect to that of layer-2. The ultimate result of this phenomenon is likely to lead to a metallic band with single spin polarization at the Fermi level (E_f), as depicted in Figure 1c, and thus the half-metallicity emerges. Furthermore, it is possible to switch the half-metallicity by reversing the FE polarization of the substrate.

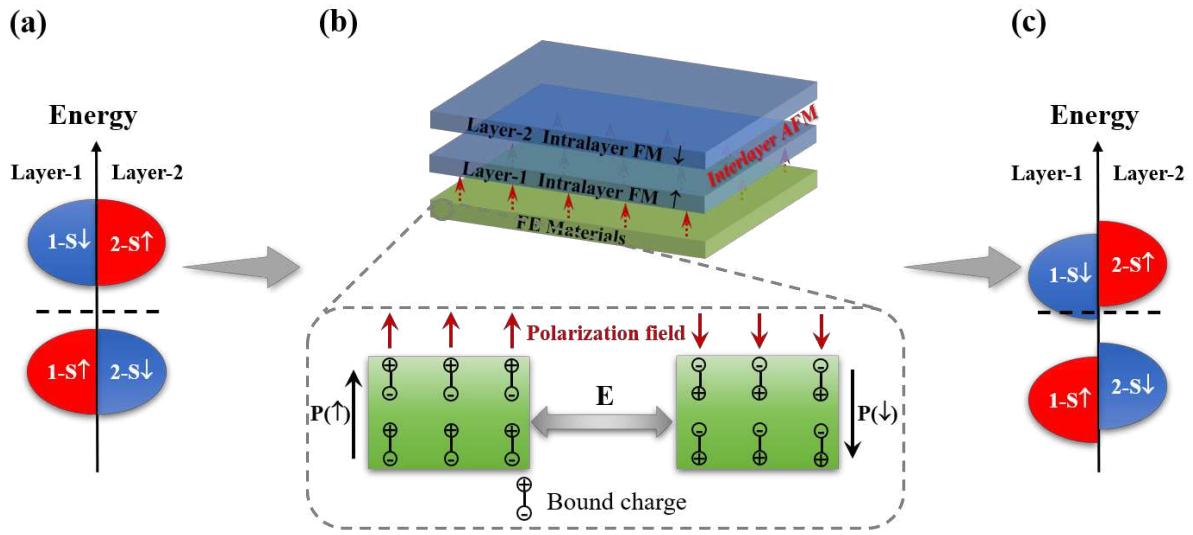

Fig. 1 Diagram of vdW heterojunction. a Schematic illustration of spin- and layer-resolved DOS for a bilayer of A-type antiferromagnet. **b** Diagram of 2D A-type antiferromagnet on FE substrate. **c** Spin- and layer-resolved DOS with half-metallicity.

Hitherto, tremendous progress in the preparation of vdW magnetic materials has provided an unprecedented opportunity for exploring and utilizing the 2D A-type AFM materials. [21-24] Very recently, the NiI_2 bilayer (bi-NiI_2) has been successfully fabricated on the h-BN substrate, which was predicted as an A-type AFM material. [25] In this work, we adopt bi-NiI_2 as the active antiferromagnet to demonstrate our above proposal. By combining bi-NiI_2 with FE In_2Se_3 with different thickness to design vdW heterostructure, the feasibility of realizing and controlling

the half-metallicity in bi-NiI_2 by electric polarization flipping is investigated. It is found that the In_2Se_3 bilayer (bi-In_2Se_3) can successfully give rise to half-metallicity in bi-NiI_2. With the reversal of polarization from upward to downward for bi-In_2Se_3, the bi-NiI_2 undergoes a transformation from half-metal to semiconductor, accompanied by a switch of easy magnetization axis from in-plane to out-of-plane direction. The nonvolatile electrical control of half-metallicity in bi-NiI_2 is the result of a combination of band shifts induced by the polarization field and selective charge transfer at the interface. Moreover, the strain effect is demonstrated as an additional route to modulate the half-metallic property and magnetic anisotropy energy (MAE). Two conceptual advanced nanodevices, a ferroelectric memory device, and a spin field effect transistor, are proposed based on the novel vdW heterostructure. These results provide an avenue to generate the switchable fully spin polarized current in AFM material, which would greatly promote the development of AFM spintronics.

2. Results and discussion

We first explore the property of pristine bi-NiI_2. To evaluate the optimized structure, six stacking patterns were constructed for bi-NiI_2, shown in Figure S1a in Supporting Information, in which the interlayer AFM and FM couplings were separately considered. The energy difference in Table S1 reveals that the AB1 configuration with A-type AFM coupling is the most energetically stable. The optimized lattice constant and interlayer distance are 3.99 and 3.45 Å, respectively. We find that the spin moment is mainly contributed by the Ni atom, and the local magnetic moment of each Ni atom is about $2\mu_B$. Figure S1b presents the band structure of the bi-NiI_2, in which a semiconductor characteristic with an indirect bandgap of 1.27 eV can be observed. The conduction band minimum (CBM) and valence band maximum (VBM) are mainly dominated by the Ni-*d* and I-*p* orbitals, respectively. From the spin- and layer-resolved DOS in Figure S1b, the spin subbands from the bottom NiI_2-1 layer and upper NiI_2-2 layer are strictly complemented, demonstrating the A-type AFM characteristic of the bi-NiI_2. A monolayer of In_2Se_3 was initially considered as the FE substrate due to its intrinsic out-of-plane FE nature. It shows a hexagonal structure with a lattice constant of 4.10 Å. The bistable polarized states are presented in Figure S2a,b, marked P↑ and P↓, which can be easily switched by a vertical electric field. The calculated band structure in Figure S2c demonstrates the

semiconductor nature of the In_2Se_3 monolayer, accompanied by a bandgap of 0.78 eV. The VBM is mainly derived from the Se-*p* orbitals, while the CBM is jointly contributed by the In-*s* and the Se-*p* orbitals, which is consistent with the previous studies. [26]

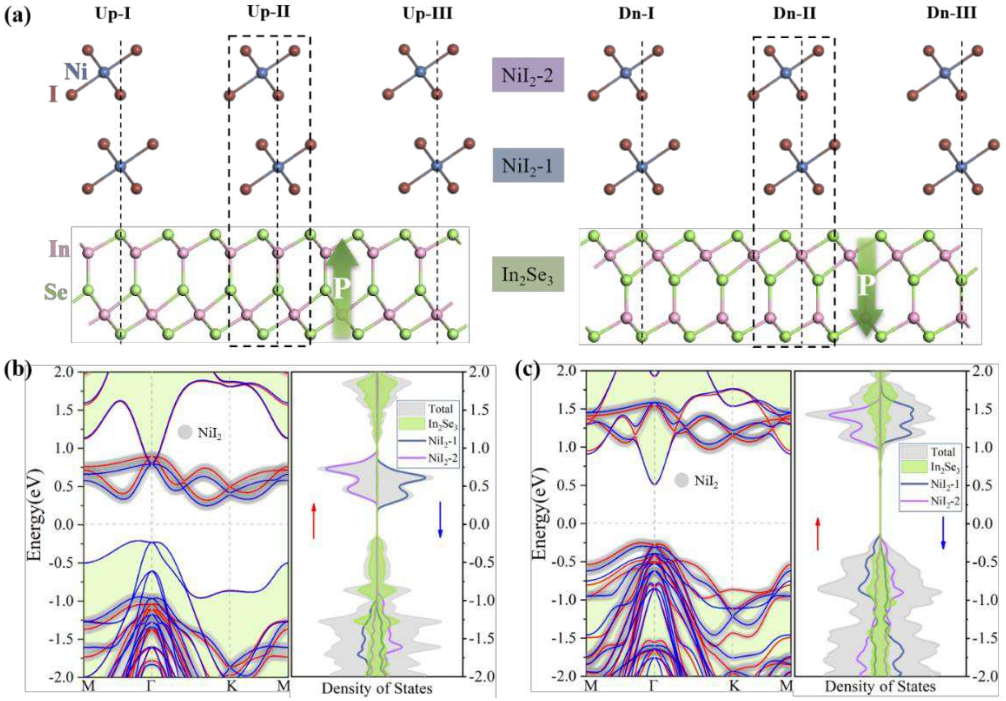

Fig. 2 bi-NiI_2/In_2Se_3 heterojunction. a Structural diagram of different stacking patterns for bi-NiI_2/In_2Se_3 heterostructure in P↑ and P↓ configurations. **b-c** Calculated band structures and DOS of bi-NiI_2/In_2Se_3 heterostructure with P↑ and P↓ states, respectively. The red and blue lines in the band structure represent spin-up and spin-down states.

A very small lattice mismatch of 2.7% between the bi-NiI_2 and the In_2Se_3 monolayer suggests a good quality vdW heterostructure can be easily constructed, which is denoted as bi-NiI_2/In_2Se_3. Here, three stacking patterns were designed for two opposite polarized states, shown in Figure 2a. Table S2 lists the relative energies of different structures. It shows the DN-II and UP-II configurations, in which the Ni atoms in the NiI_2-1 layer located above the upper In atom of the adjacent In_2Se_3 monolayer, are energetically lower than the other configurations. More importantly, the A-type AFM coupling of bi-NiI_2 was maintained in the vdW heterostructure. The obtained interlayer distances between bi-NiI_2 and In_2Se_3 monolayer are 3.20 and 3.16Å for P↑ and P↓ cases, respectively. This small difference implies that polarization switching has a negligible effect on the interlayer distance. Besides, the structural stability of vdW heterostructure was evaluated by the calculation of the formation energies, which is

defined as $E_{form} = E(\text{bi-NiI}_2/\text{In}_2\text{Se}_3) - E(\text{bi-NiI}_2) - E(\text{In}_2\text{Se}_3)$, where the $E(\text{bi-NiI}_2/\text{In}_2\text{Se}_3)$, $E(\text{bi-NiI}_2)$ and $E(\text{In}_2\text{Se}_3)$ are total energies of bi-NiI_2/In_2Se_3 vdW heterostructure, individual bi-NiI_2 and In_2Se_3 layers, respectively. The calculated formation energy is about -1.40eV, suggesting the feasibility of experimental preparation of such vdW heterostructure. Based on the formation energy and interlayer distance, the interlayer vdW interaction in heterostructure is further demonstrated.

Then the electronic properties of bi-NiI_2/In_2Se_3 vdW heterostructures were investigated. Figure 2b,c present the calculated band structures and DOS of the heterostructure. For the P↑ configuration, the band degeneracy of the bi-NiI_2 was removed due to different degrees of energy level shift for NiI_2-1 and NiI_2-2 layers. The spin splitting could reach up to about 73.4 meV. The CBM and VBM were dominated by the bi-NiI_2 and the In_2Se_3 monolayer, respectively, indicating that the bi-NiI_2/In_2Se_3 belongs to a typical staggered-gap (type II) heterostructure. The conduction band nearest to the E_f in the spin-down channel is associated with the NiI_2-1 layer. With respect to the pristine bi-NiI_2, the energy band of bi-NiI_2 in the heterostructure moved significantly down relative to the E_f when the electric polarization of the FE substrate is upward. Once the polarization is reversed to the P↓ state, the band structure of the heterostructure undergoes a dramatic change, shown in Figure 2c. Although the type-II band alignment behavior is preserved, the domination components for the CBM and VBM changed significantly since a relative displacement of the energy levels of the bi-NiI_2 and the In_2Se_3 monolayer were triggered by the polarization flipping. In addition, the spin splitting in the bi-NiI_2 was reduced to about 51.5 meV. The valance band edge close to the E_f in the spin-up channel was also contributed by the NiI_2-1 layer. In general, despite the spin splitting and band shift induced by the FE polarization, the energy bands contributed by the bi-NiI_2 and the In_2Se_3 monolayer in the vdW heterostructure were very similar to their pristine cases, which indicates that there is no obvious hybridization between the AFM bilayer and FE substrate. Although the In_2Se_3 monolayer would not bring about qualitative change for the electronic property of bi-NiI_2, the generated electric polarization indeed drives the downward shift of energy level of bi-NiI_2, which offers an opportunity to further manipulate the electronic property by enhancing polarization field.

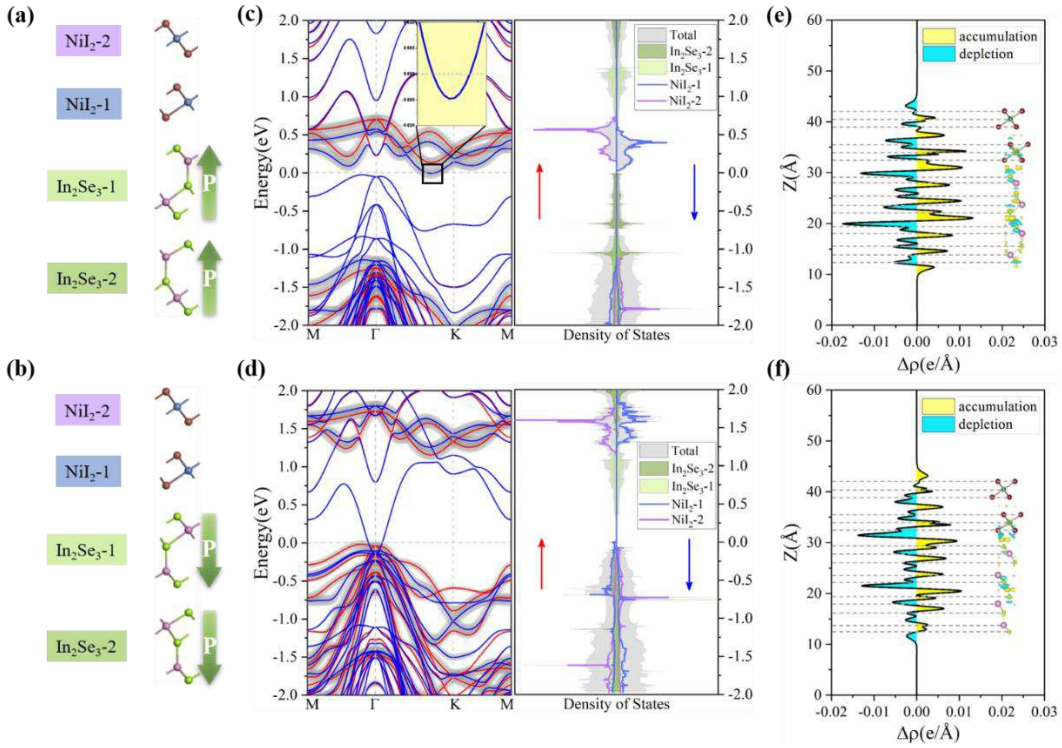

Fig. 3 bi-NiI_2/bi-In_2Se_3 heterojunction. Structural diagrams **(a,b)**, calculated band structures and DOSs **(c,d)**, and differential charge distributions **(e,f)** of bi-NiI_2/bi-In_2Se_3 heterostructure in P↑↑ and P↓↓ configurations, respectively. The red and blue lines in band structures represent spin-up and spin-down states.

To verify the above conception, one more In_2Se_3 layer was added at the bottom of bi-NiI_2/In_2Se_3. This new vdW heterostructure is named bi-NiI_2/bi-In_2Se_3. Here, for simplicity, two different polar configurations were taken into account for the bi-In_2Se_3, *i.e.* the polarization directions of FE layers were both pointing upward (P↑↑) or downward (P↓↓). The stacking pattern of the bi-In_2Se_3 was also optimized and shown in Figure S2d. It revealed that in the most stable configuration, the upper In atom in the In_2Se_3-1 layer is vertically aligned with the upper Se atom in the In_2Se_3-2 layer. Figures 3a,b show the geometric structures of bi-NiI_2/bi-In_2Se_3 in the P↑↑ and P↓↓ configurations. The calculated formation energy of the bi-NiI_2/bi-In_2Se_3 is about 0.09 eV, suggesting that such a complex heterostructure is promising to be produced. The interlayer distance at the NiI_2-In_2Se_3 interface is insensitive to the addition of the second In_2Se_3 layer, and it is found to be 3.20 and 3.19 Å for the P↑↑ and P↓↓ cases, respectively. Remarkably, the A-type AFM ground state of the bi-NiI_2 is persisted, which is immune to the polarization

direction of the substrate, and the energy differences between AFM and FM states for the P↑↑ and P↓↓ cases are 9.68 and 10.68 eV/u.c., respectively.

The effect of the bi-In_2Se_3 on the electronic property of the bi-NiI_2 was also investigated. The spin-resolved band structures and DOSs of bi-NiI_2/bi-In_2Se_3 heterostructures are plotted in Figure 3c,d. For the P↑↑ state, the spin splitting of the energy band for the bi-NiI_2 was increased to 138.7 meV because of the enhanced polarization field from the bilayer of the FE substrate, which is about double that of bi-NiI_2/In_2Se_3. More interestingly, the E_f passes through the spin-down conduction band edge, which forms an interesting band structure with half-metallicity, shown in Figure 3c. From the DOS analysis, the electronic states at the E_f were dominated by the contribution from the NiI_2-1 layer, while the NiI_2-2 layer remained its semiconductor property. To be brief, the bi-NiI_2 possesses the AFM half-metallicity under the action of the upward FE polarization from the substrate, which makes the generation of fully polarized current possible. By flipping the electric polarization of bi-In_2Se_3, we find that the energy bands associated with the bi-NiI_2 shifted upward relative to the E_f, while the spin splitting was decreased to 98.9 meV, as depicted in Figure 3d. Although the valance band edge is near the E_f, no intersection was observed, implying the disappearance of the half-metallicity and recovery of the semiconductor for the bi-NiI_2. In addition, the E_f cut through the energy band contributed by bi-In_2Se_3, and thus the FE substrate was endowed with the metallicity. Despite the presence of the conductive state for both P↑↑ and P↓↓ cases, the produced currents in heterostructure were distinctly different: the former is fully spin polarized and localized in the bi-NiI_2, while the latter is spin depolarized and existed in the bi-In_2Se_3 substrate.

Next, we discuss the underlying physics for the electrically controlled half-metallicity in the AFM bi-NiI_2. The In_2Se_3 monolayer with out-of-plane FE polarization can produce an external polarization field. When the bi-NiI_2 was deposited on In_2Se_3 monolayer, the polarization field would act upon the AFM bilayer. The distinct spatial position of NiI_2-1 and NiI_2-2 layers determines that their potential energies were different, shown in Figure S3. Thus the unequal band shift and band spin splitting are expected. The potential energy differences of the two NiI_2 layers were 0.24 and 0.16eV for P↑ and P↓ cases, respectively, which results in different degrees of spin splitting with the opposite polarized states. By increasing the thickness of the FE layer, the polarization field was enhanced correspondingly, which improved the

degrees of band shift and spin-splitting. For the P↑↑ case, the enhanced polarization field offered a prerequisite to realizing the half-metallicity for bi-NiI_2, while the charge transfer at the NiI_2-In_2Se_3 interface played a decisive role. The three-dimensional (3D) and plane-integrated differential charge distribution of bi-NiI_2/bi-In_2Se_3 are presented in Figure 3e,f. The charge transfer was mainly located at the NiI_2-In_2Se_3 and the In_2Se_3-In_2Se_3 interfaces, whereas it is almost negligible between the NiI_2-1 and the NiI_2-2 layers. This can be explained by comparing the work functions of the In_2Se_3 and the NiI_2 pristine layers. Since the In_2Se_3 layer is highly polarized, the calculated work functions on the two sides of the sample are different, *i.e.* W_1=5.24 eV for the Se_+ surface and W_2=6.03 eV for the Se_- surface. However, for the nonpolar NiI_2 monolayer, the work function shows a single value of W = 5.62 eV. Hence, the obtained work functions satisfy the relationship of $W_1<W<W_2$. With an upward polarization direction, the electrons would transfer from the In_2Se_3-2 to the NiI_2-1, shown in Figure 3e. The charge transfer will result in the electrons depletion at the upper surface of In_2Se_3-2 and the electron accumulation at the lower surface of NiI_2-1, respectively. The extra electrons in the NiI_2-1 layer will partially occupy the conduction band edge, leading to the phenomenon of electron doping. Therefore, the half-metallicity in the bi-NiI_2 is the synergistic result of the polarization field induced variation of band alignment and charge redistribution induced electron doping. With the reversal of the electric polarization, the electrons in the NiI_2-1 layer tend to transfer to the In_2Se_3-2 layer due to $W<W_2$, see Figure 3f, which endows the bi-In_2Se_3 substrate with electron doping and conductive state. On the other hand, the work function at the In_2Se_3-In_2Se_3 interface is invariably different, and thus the charge transfer associated with the polarization direction is inevitable. The inappreciable interlayer charge transfer between the NiI_2 layers can be attributed to the identical work function between the two layers.

For the AFM materials, the manipulation of easy magnetization axis is of significance and has attracted great attention. [27-32] Thus it is important to identify the response of the easy magnetization axis of bi-NiI_2 to the polarization switching. The MAE of the bi-NiI_2/bi-In_2Se_3 heterostructure was also calculated. The result indicates that the magnetization axis of the bi-NiI_2 is isotropic within the *xy* plane, regardless of the polarization direction of the FE substrate. Figure 4a,b show the MAE associated with polar angle (θ). It turns out that the easy magnetization axis for the P↑↑ and P↓↓ cases are demonstrated to be in-plane and out-of-plane,

respectively. Hence, the polarization flipping of substrate can effectively switch the easy magnetization axis of the bi-NiI_2. Additionally, the magnitude of MAE for the bi-NiI_2/bi-In_2Se_3 is considerably larger than those of Sc_2CO_2/VSe_2 and bi-CrI_3/Sc_2CO_2 heterostructures. [33,34] With these outstanding advantages, the bi-NiI_2/bi-In_2Se_3 heterostructure shows promising potential for the application as an efficient nonvolatile memory.

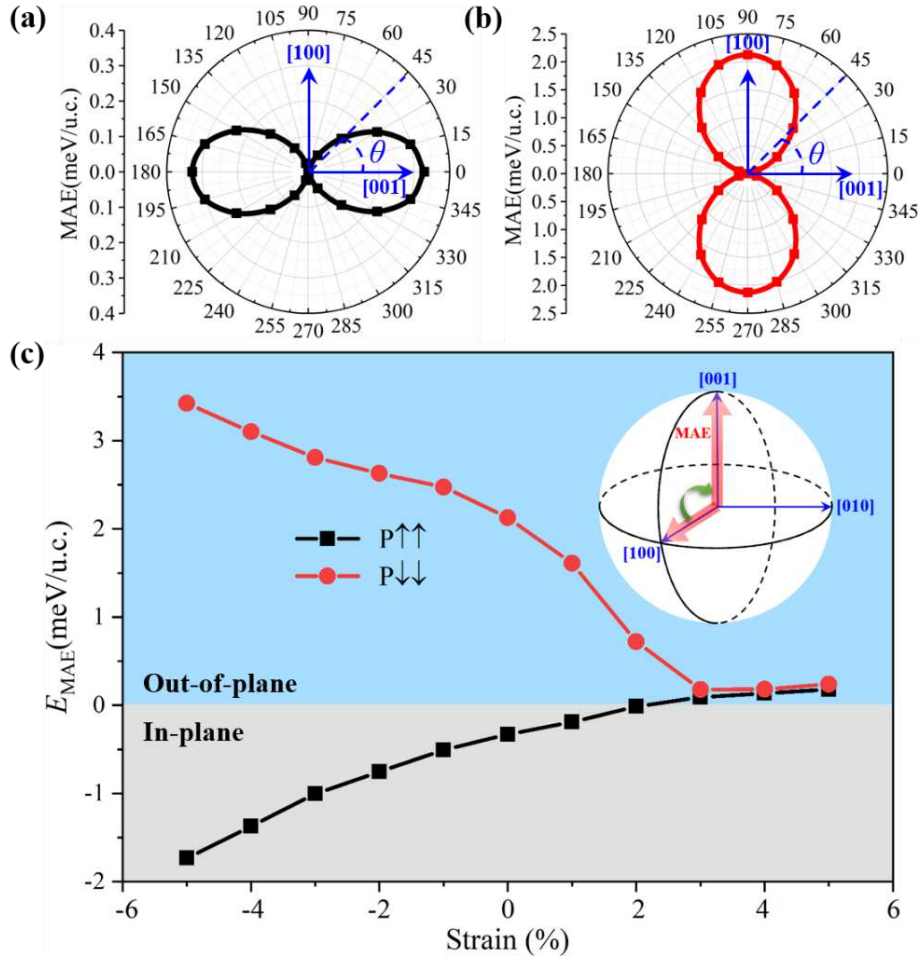

Fig. 4 MAE and stress regulation. a-b Polar angel (θ) dependence of MAE with *a-c* plane for P↑↑ and P↓↓ cases, respectively. **c** Variation of E_{MAE} as a function of biaxial strain for P↑↑ and P↓↓ cases.

As mentioned above, the upward FE polarization can induce the electron doping for bi-NiI_2, while the downward FE polarization drives the valance band edge of the bi-NiI_2 extremely close to the E_f. Such electronic properties suggest that external means, such as in-plane biaxial strain, may further tailor the electronic behavior of the heterostructure. Figure S4 shows the band structures of heterostructure under different biaxial strains. When the compressive strain

was applied, the energy band dispersion becomes more extended because of bond length shortening. This would enhance the electron doping into the bi-NiI_2 in the P↑↑ configuration, which will in turn increase the conductivity of the half-metallic bi-NiI_2. Meanwhile, for the P↓↓ case, the valance band edge of the bi-NiI_2 shifts upward continuously with the increase of the compressive strain, and finally intersects with the E_f at -3% of strain, leading to a hole doping induced half-metallicity. Such half-metallicity is also stemmed from the NiI_2-1 layer, but determined by the spin-up state. Thus, within an appropriate range of the compressive strain, the half-metallicity of the bi-NiI_2 becomes independent of polarization flipping, whereas the reversal of the polarization can effectively switch the type of charge carrier and the spin orientation of the fully spin polarized current. On the other hand, the tensile strain enlarges the bond length and improves the localization of energy bands. Once the tensile strain was implemented, the bi-NiI_2 would restore the semiconductor property due to the depletion of the doped electrons. Hence, for developing spintronics applications, the manipulation with compressive strain is more effective for providing better spin control. The evolution of the MAE was also studied as a function of the biaxial strain. The energy difference between the magnetization in *x* (100) and *z* (001) directions was calculated, which is defined as $E_{MAE} = E_{100} - E_{001}$. Figure 4c illustrates the variation of E_{MAE} for the P↑↑ and P↓↓ cases. As the compressive strain increases, the magnitude of E_{MAE} has also been enhanced accordingly. The easy magnetization axis of heterostructure in opposite polarization configurations was unchanged, which is consistent with the equilibrium state. Conversely, the E_{MAE} decrease with the increase of the tensile strain. Remarkably, the easy magnetization axis of heterostructure in the P↑↑ configuration was switched from in-plane to out-of-plane when the tensile strain was larger than 3%. In other word, under this condition, the easy magnetization axis was independent of the polarization direction and always aligned along the z direction.

The results have revealed that the heterostructure possesses the capacity of controlling the half-metallicity by FE polarization, which provides a promising opportunity for designing new-type ferroelectric memory devices. Here, a prototype of a memory device is proposed based on the heterostructure, shown in Figure 5a. The electric polarization in the bi-In_2Se_3 is switched by an independent voltage V_A, and the bi-NiI_2 as the conducting channel is contacted with the source/drain. When the FE substrate is in P↑↑ configuration, the electron would travel through

the channel layer with 100% spin polarization, due to the half-metallicity of the bi-NiI_2. Such conductive state is denoted "1" or "ON" state of the device, shown in Figure 5b. By flipping the FE substrate to a P↓↓ configuration, the bi-NiI_2 becomes a semiconductor and the traveling of electrons is forbidden. This corresponds to the "0" or "OFF" state of the device, shown in Figure 5c. In this scenario, the data reading process is accessible by converting the FE polarization state of bi-In_2Se_3 into conducting state of bi-NiI_2 and detecting it, which can effectively avoid the destructive effect caused by detecting the polarized state. Furthermore, the scheme in Figure 5a can also be adopted into spin field-effect transistors (SFETs). Different from a traditional semiconductor transistor with modulating the charge populations, the working principle of bi-NiI_2/bi-In_2Se_3 heterostructure based SFET is manipulating the band structure of the AFM bilayer *via* controlling the FE polarization of the substrate. Thereby, this SFET not only has the advantage of rapid response but more importantly, the regulation between different states is nonvolatile. Therefore, the SFET can be used in high performance and low power consumption devices.

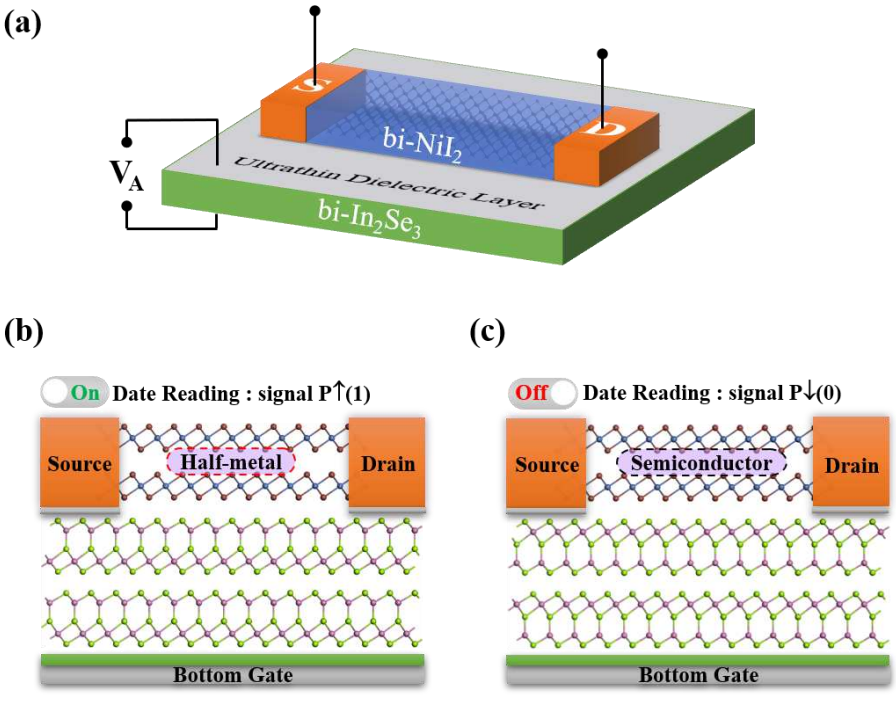

Fig. 5 Device prototype and schematic diagram. a Prototypes of the ferroelectric memory device and spin-field effect transistor based on the bi-NiI_2/bi-In_2Se_3 heterostructure. **b-c** Operation principle of ferroelectric memory device whose data writing depends on FE bi-In_2Se_3 and data reading is based on the different electric signal.

To realize above device functions, switching the polarization of the FE substrate *via* external electric field is a very vital tache. However, the result has revealed that the FE bi-In_2Se_3 is also conductive in the heterostructure when the electric polarization was downward. For a metallic FE material, the polarization is difficult to be switched since the required voltage bias will produce a high electrical current rather than changing the structural polarity. Inspired by the recently successful case of the polarization reversal in the FE semimetal WTe_2, [35] it is possible to eliminate the electrical current by inserting a dielectric layer into the bi-NiI_2/bi-In_2Se_3 heterostructure, which might be able to achieve the polarization switching *via* an external electric field. In addition, the FE bistability of bi-NiI_2/bi-In_2Se_3 was also investigated, since it is closely associated with device performance. As a matter of fact, the polarization reversal in the FE In_2Se_3 layer requires undergoing an intermediate antiferroelectric (AFE) state. Thus the heterostructure in the AFE configuration was constructed, shown in Figure S5. By calculating the total energy, we find that the total energy of the AFE configuration is 2.05 eV/u.c. higher than the P↑↑ and P↓↓ cases. Therefore, the bi-NiI_2/bi-In_2Se_3 heterostructure offers sufficient bistability for the device application.

3. Conclusions

In summary, we have proposed vdW heterostructures formed by A-type AFM bi-NiI_2 and FE In_2Se_3 with different thickness. With first-principle calculations, half-metallicity was obtained from the bi-NiI_2 proximate to the bi-In_2Se_3. The polarization flipping of bi-In_2Se_3 from upward to downward would convert the bi-NiI_2 from half-metal to semiconductor. Meanwhile, the easy magnetization axis of bi-NiI_2 also undergoes a transition from the in-plane to the out-of-plane direction. It shows that the cooperation between the band shift induced by the polarization field and selective charge transfer at the interface is responsible for achieving the nonvolatile half-metallicity. The half-metallic behavior and the MAE in the heterostructure can be further adjusted by introducing strain. The prototypes of a ferroelectric memory device and SFET are designed using the vdW heterostructure. This works offers a possible scheme to achieve and control the half-metallicity in 2D A-type antiferromagnet. It opens opportunities for new spintronic devices.

4. Methods

First principles calculations were performed within the framework of density functional theory (DFT) by the projector-augmented wave (PAW) method, [36] as implemented in the Vienna ab initio simulation package (VASP). [37,38] The Perdew-Burke-Ernzerhof generalized gradient approximation (PBE-GGA) was adopted to describe the exchange and correlation functional. [39,40] An effective Hubbard *U* parameter of 5.0 eV was included for the 3*d* orbitals of the Ni element. [25] The kinetic energy cutoff of 500 eV for the plane-wave basis set was used throughout the calculation. Structural relaxations were carried out until the residual force on each atom wasless than 0.005 eV/Å, and the energy convergence criteria of 10^{-6} eV was employed. The Brillouin zone was sampled using a Γ-centered Monkhorst-Pack scheme with 17 ×17 × 1. A vacuum layer with a thickness larger than 30 Å was set to eliminate interactions between periodic images. The interlayer vdW interaction is described by the DFT-D3 method. [41,42]

Data Availability

The authors declare that the main data supporting the findings of this study are available within the article and its Supplementary Information files.

References

1. Jungwirth, T., Marti, X., Wadley, P. & Wunderlich, J. Antiferromagnetic spintronics. *Nat. Nanotechnol.* **11**, 231-241 (2016).
2. Jungwirth, T.*, et al.* The multiple directions of antiferromagnetic spintronics. *Nat. Phys.* **14**, 200-203 (2018).
3. Baltz, V.*, et al.* Antiferromagnetic spintronics. *Rev. Mod. Phys.* **90**(2018).
4. Železný, J., Wadley, P., Olejník, K., Hoffmann, A. & Ohno, H. Spin transport and spin torque in antiferromagnetic devices. *Nat. Phys.* **14**, 220-228 (2018).
5. Baldrati, L.*, et al.* Mechanism of N\'eel Order Switching in Antiferromagnetic Thin Films Revealed by Magnetotransport and Direct Imaging. *Phys. Rev. Lett.* **123**, 177201

(2019).

6. Holzberger, S., Schuh, T., Blügel, S., Lounis, S. & Wulfhekel, W. Parity Effect in the Ground state Localization of Antiferromagnetic Chains Coupled to a Ferromagnet. *Phys. Rev. Lett.* **110**, 157206 (2013).
7. Xu, Y., Wang, S. & Xia, K. Spin-Transfer Torques in Antiferromagnetic Metals from First Principles. *Phys. Rev. Lett.* **100**, 226602 (2008).
8. Hu, X. Half-Metallic Antiferromagnet as a Prospective Material for Spintronics. *Adv. Mater.* **24**, 294-298 (2012).
9. Tong, J.*, et al.* High and reversible spin polarization in a collinear antiferromagnet. *Appl. Phys. Rev.* **7**, 031405 (2020).
10. Wadley, P.*, et al.* Electrical switching of an antiferromagnet. *Science* **351**, 587-590 (2016).
11. Gong, S.J.*, et al.* Electrically induced 2D half-metallic antiferromagnets and spin field effect transistors. *Natl Acad. Sci. USA* **115**, 8511-8516 (2018).
12. Geim, A.K. & Grigorieva, I.V. Van der Waals heterostructures. *Nature* **499**, 419-425 (2013).
13. Gong, C. & Zhang, X. Two-dimensional magnetic crystals and emergent heterostructure devices. *Science* **363**, eaav4450 (2019).
14. Novoselov, K.S., Mishchenko, A., Carvalho, A. & Castro Neto, A.H. 2D materials and van der Waals heterostructures. *Science* **353**, aac9439 (2016).
15. Gong, C., Kim, E.M., Wang, Y., Lee, G. & Zhang, X. Multiferroicity in atomic van der Waals heterostructures. *Nat. Commun.* **10**, 2657 (2019).
16. Li, Z. & Zhou, B. Theoretical investigation of nonvolatile electrical control behavior by ferroelectric polarization switching in two-dimensional MnCl3/CuInP2S6 van der Waals heterostructures. *J. Mater. Chem. C* **8**, 4534-4541 (2020).
17. Liu, W.-R.*, et al.* Magnetic anisotropy and ferroelectric-driven magnetic phase transition in monolayer Cr2Ge2Te6. *Nanoscale* **14**, 3632-3643 (2022).
18. Pei, Q., Zhou, B., Mi, W. & Cheng, Y. Triferroic Material and Electrical Control of Valley Degree of Freedom. *ACS Appl. Mater. Inter.* **11**, 12675-12682 (2019).
19. Zhao, Y., Zhang, J.J., Yuan, S. & Chen, Z. Nonvolatile Electrical Control and

Heterointerface-Induced Half-Metallicity of 2D Ferromagnets. *Adv. Funct. Mater.* **29**, 1901420 (2019).

20. Sun, W., Wang, W., Chen, D., Cheng, Z. & Wang, Y. Valence mediated tunable magnetism and electronic properties by ferroelectric polarization switching in 2D FeI2/In2Se3 van der Waals heterostructures. *Nanoscale* **11**, 9931-9936 (2019).
21. Bonilla, M.*, et al.* Strong room-temperature ferromagnetism in VSe2 monolayers on van der Waals substrates. *Nat. Nanotechnol.* **13**, 289-293 (2018).
22. Fei, Z.*, et al.* Two-dimensional itinerant ferromagnetism in atomically thin Fe3GeTe2. *Nat. Mater.* **17**, 778-782 (2018).
23. Gong, C.*, et al.* Discovery of intrinsic ferromagnetism in two-dimensional van der Waals crystals. *Nature* **546**, 265-269 (2017).
24. Huang, B.*, et al.* Layer-dependent ferromagnetism in a van der Waals crystal down to the monolayer limit. *Nature* **546**, 270-273 (2017).
25. Liu, H.*, et al.* Vapor Deposition of Magnetic Van der Waals NiI2 Crystals. *ACS Nano* **14**, 10544-10551 (2020).
26. Tian, H.*, et al.* Band structure engineering of van der Waals heterostructures using ferroelectric clamped sandwich structures. *Phys. Rev. B* **103**(2021).
27. Fukami, S., Zhang, C., DuttaGupta, S., Kurenkov, A. & Ohno, H. Magnetization switching by spin–orbit torque in an antiferromagnet–ferromagnet bilayer system. *Nat. Mater.* **15**, 535-541 (2016).
28. Kurenkov, A., Zhang, C., DuttaGupta, S., Fukami, S. & Ohno, H. Device-size dependence of field-free spin-orbit torque induced magnetization switching in antiferromagnet/ferromagnet structures. *Appl. Phys. Lett.* **110**, 092410 (2017).
29. Oh, Y.-W.*, et al.* Field-free switching of perpendicular magnetization through spin–orbit torque in antiferromagnet/ferromagnet/oxide structures. *Nat. Nanotechnol.* **11**, 878-884 (2016).
30. Peng, S.*, et al.* Exchange bias switching in an antiferromagnet/ferromagnet bilayer driven by spin–orbit torque. *Nat. Electron.* **3**, 757-764 (2020).
31. Wang, Y.*, et al.* Magnetization switching by magnon-mediated spin torque through an antiferromagnetic insulator. *Science* **366**, 1125-1128 (2019).

32. Zhang, P.X.*, et al.* Spin-orbit torque in a completely compensated synthetic antiferromagnet. *Phys. Rev. B* **97**, 214403 (2018).

33. Lu, Y.*, et al.* Artificial Multiferroics and Enhanced Magnetoelectric Effect in van der Waals Heterostructures. *ACS Appl. Mater. Inter.* **12**, 6243-6249 (2020).

34. Jiang, P.*, et al.* Ferroelectric control of electron half-metallicity in A-type antiferromagnets and its application to nonvolatile memory devices. *Phys. Rev. B* **102**(2020).

35. Sharma, P.*, et al.* A room-temperature ferroelectric semimetal. *Sci. Adv.* **5**, eaax5080(2019).

36. Kresse, G. & Joubert, D. From ultrasoft pseudopotentials to the projector augmented-wave method. *Phys. Rev. B* **59**, 1758-1775 (1999).

37. Kresse, G. & Furthmüller, J. Efficient iterative schemes for ab initio total-energy calculations using a plane-wave basis set. *Phys. Rev. B* **54**, 11169-11186 (1996).

38. Kresse, G. & Hafner, J. Ab initio molecular-dynamics simulation of the liquid-metal–amorphous-semiconductor transition in germanium. *Phys. Rev. B* **49**, 14251-14269 (1994).

39. Grimme, S. Semiempirical GGA-type density functional constructed with a long-range dispersion correction. *J. Comput. Chem.* **27**, 1787-1799 (2006).

40. Perdew, J.P. & Wang, Y. Accurate and simple analytic representation of the electron-gas correlation energy. *Phys. Rev. B* **45**, 13244-13249 (1992).

41. Grimme, S., Antony, J., Ehrlich, S. & Krieg, H. A consistent and accurate ab initio parametrization of density functional dispersion correction (DFT-D) for the 94 elements H-Pu. *J. Chem. Phys.* **132**, 154104 (2010).

42. Grimme, S., Ehrlich, S. & Goerigk, L. Effect of the damping function in dispersion corrected density functional theory. *J. Comput. Chem.* **32**, 1456-1465 (2011).

Acknowledgements

This work was supported by the National Natural Science Foundation of China (Grant Nos. 12004137 and 11974145), the Key Research and Development Program of Shandong Province

(No. 2019JZZY010313), and Natural Science Foundation of Shandong Province (Grant Nos. ZR2020QA052 and ZR2020ZD28)

Author Contributions

S. L. conceived the idea and designed the project, Y. W. performed the calculations and wrote the paper with the help of S. L. and W. J., Q. C. participated in the discussion and writing of device applications. X. X., X. Z. and Y. L. supervised the project. All authors analyzed the data and contributed to the discussions of the results.

Corresponding Authors

*E-mail: sdy_liss@ujn.edu.cn

*E-mail: liyanlu@sdu.edu.cn

Conflicts of interest

There are no conflicts of interest to declare

Supplementary Files

This is a list of supplementary files associated with this preprint. Click to download.

- SupprotingInformation.pdf